

PAPER

Ultra-small carbon fiber electrode recording site optimization and improved *in vivo* chronic recording yield

To cite this article: Elissa J Welle *et al* 2020 *J. Neural Eng.* **17** 026037

View the [article online](#) for updates and enhancements.



The Department of Bioengineering at the University of Pittsburgh Swanson School of Engineering invites applications from accomplished individuals with a PhD or equivalent degree in bioengineering, biomedical engineering, or closely related disciplines for an open-rank, tenured/tenure-stream faculty position. We wish to recruit an individual with strong research accomplishments in Translational Bioengineering (i.e., leveraging basic science and engineering knowledge to develop innovative, translatable solutions impacting clinical practice and healthcare), with preference given to research focus on neuro-technologies, imaging, cardiovascular devices, and biomimetic and biorobotic design. It is expected that this individual will complement our current strengths in biomechanics, bioimaging, molecular, cellular, and systems engineering, medical product engineering, neural engineering, and tissue engineering and regenerative medicine. In addition, candidates must be committed to contributing to high quality education of a diverse student body at both the undergraduate and graduate levels.

[CLICK HERE FOR FURTHER DETAILS](#)

To ensure full consideration, applications must be received by June 30, 2019. However, applications will be reviewed as they are received. Early submission is highly encouraged.



PAPER

Ultra-small carbon fiber electrode recording site optimization and improved *in vivo* chronic recording yield

Elissa J Welle¹ , Paras R Patel¹ , Joshua E Woods², Artin Petrossians³ , Elena della Valle¹ , Alexis Vega-Medina^{4,5}, Julianna M Richie¹, Dawen Cai^{4,5,6} , James D Weiland^{1,3,7}  and Cynthia A Chestek^{1,2,5,7,8} 

¹ Department of Biomedical Engineering, University of Michigan, Ann Arbor, MI, United States of America

² Department of Electrical Engineering and Computer Science, University of Michigan, Ann Arbor, MI, United States of America

³ Platinum Group Coatings, Pasadena, CA, United States of America

⁴ Department of Cell and Developmental Biology, University of Michigan, Ann Arbor, MI, United States of America

⁵ Neuroscience Graduate Program, University of Michigan, Ann Arbor, MI, United States of America

⁶ Biophysics, University of Michigan, Ann Arbor, MI, United States of America

⁷ Robotics Graduate Program, University of Michigan, Ann Arbor, MI, United States of America

⁸ Author to whom any correspondence should be addressed.

E-mail: cchestek@umich.edu

Keywords: carbon electrodes, neural probes, neural recording, electrode surface modification, recording yield, electrodeposited platinum iridium

Supplementary material for this article is available [online](#)

Abstract

Objective. Carbon fiber electrodes may enable better long-term brain implants, minimizing the tissue response commonly seen with silicon-based electrodes. The small diameter fiber may enable high-channel count brain-machine interfaces capable of reproducing dexterous movements. Past carbon fiber electrodes exhibited both high fidelity single unit recordings and a healthy neuronal population immediately adjacent to the recording site. However, the recording yield of our carbon fiber arrays chronically implanted in the brain typically hovered around 30%, for previously unknown reasons. In this paper we investigated fabrication process modifications aimed at increasing recording yield and longevity. **Approach.** We tested a new cutting method using a 532nm laser against traditional scissor methods for the creation of the electrode recording site. We verified the efficacy of improved recording sites with impedance measurements and *in vivo* array recording yield. Additionally, we tested potentially longer-lasting coating alternatives to PEDOT:pTS, including PtIr and oxygen plasma etching. New coatings were evaluated with accelerated soak testing and acute recording. **Main results.** We found that the laser created a consistent, sustainable $257 \pm 13.8 \mu\text{m}^2$ electrode with low 1 kHz impedance ($19 \pm 4 \text{ k}\Omega$ with PEDOT:pTS) and low fiber-to-fiber variability. The PEDOT:pTS coated laser cut fibers were found to have high recording yield in acute (97% > 100 μV_{pp} , N = 34 fibers) and chronic (84% > 100 μV_{pp} , day 7; 71% > 100 μV_{pp} , day 63, N = 45 fibers) settings. The laser cut recording sites were good platforms for the PtIr coating and oxygen plasma etching, slowing the increase in 1 kHz impedance compared to PEDOT:pTS in an accelerated soak test. **Significance.** We have found that laser cut carbon fibers have a high recording yield that can be maintained for over two months *in vivo* and that alternative coatings perform better than PEDOT:pTS in accelerated aging tests. This work provides evidence to support carbon fiber arrays as a viable approach to high-density, clinically-feasible brain-machine interfaces.

1. Introduction

Brain-machine interfaces (BMIs) translate neural dynamics into therapeutic technologies for the

restoration of movement and sensation to critically disabled patients [1]. Exciting recent proof of concept demonstrations using neural interfaces to treat neurological disorders include multi-degree-of-freedom

control of paralyzed limbs using functional electrical stimulation [2, 3], novel prosthetic hands with tens of degrees of freedom [4, 5], more widely available upper limb exoskeletons [6], and systems of implantable devices with realistic power consumption for neural recording with high channel count [7–9]. Future BMIs will aim to translate movement intention into more naturalistic or complex movements, such as control of individual fingers [10–13].

BMI research relies heavily upon the Utah array [14], the only multi-shank electrode approved for clinical use, for decoding intended movements from motor cortex [2, 3, 15–19]. High density neural electrodes have also been applied to other biological systems to restore complex functions, such as closed-loop bladder control [20], vision restoration [21–23], or memory encoding [24]. However, Utah arrays and other conventional silicon-based arrays are associated with a number of limiting factors that may inhibit a dramatic expansion of channels or increase in longevity. For example, it has been observed that the number of channels on silicon-based arrays capable of recording neural activity, termed recording yield, decreases over time and is associated with a decrease in the amplitude of recorded action potentials [25, 26]. Experiments using Michigan-style silicon arrays typically begin with a recording yield of 50% or less in the first week [27–29] and with amplitudes of 150 μV or lower. This may be due in part to an electrode configuration that spans multiple cortical layers containing neurons. However, any decrease in yield or amplitude may threaten the utility of the entire array. In BMI experiments, decode performance can be maintained by using threshold crossings instead of well-isolated action potentials [25], common average referencing [29], and high frequency field potentials [30] that may reflect underlying spiking activity [31]. However, the inability to record individual spikes may limit the creation of intuitive neural prosthetics. Thus, there is a pressing need for robust, stable, high-density neural interfaces.

Tissue damage and inflammation may play a role in the degradation of electrode performance over time. There is damage during insertion of conventional silicon-based electrodes, often disrupting the blood brain barrier and triggering an immune response [32]. Once inserted, an electrode's presence often induces an inflammatory tissue response in the surrounding tissue that can be much larger than the electrode footprint itself [33]. Chronic inflammation leads to fibrotic encapsulation, distancing the recording electrode from healthy neurons [34, 35]. Finally, the lining of the encapsulation is composed of activated macrophages and foreign body giant cells that produce enzymes and reactive oxygen species, which contribute to electrode degradation [36]. Therefore, in order to maintain high quality signals on all channels over time, it is critically important to minimize tissue damage and inflammation.

With the overall goal of minimizing scarring, groups have developed electrodes that are softer, smaller, or both. Soft electrodes more closely align with the brain's Young's modulus [37] and show some improvement in histological results. Most soft devices have been similar in size to conventional probes, however [38], which is not sufficient by itself to eliminate the immune response. Very little scarring has been observed near soft probes that have neuron-sized dimensions [39–41]. However, like larger soft electrodes, small-footprint devices may need to rely on an insertion shuttle, such as an injection needle [39], microwire [42, 43], or a temporary stiffening agent [44], which adds to surgical complexity.

Multiple groups have made cellular scale probes out of higher Young's modulus materials, such as carbon fiber [45–52], silicon carbide [53], or glass [54], that can be driven directly into the brain. At these size scales, even stiff materials are quite flexible and cause much less scarring than conventionally sized probes [28]. However, most small-footprint devices were developed recently and have not been rigorously evaluated in terms of recording yield in long term studies comparable to the Utah array. For example, a recent white paper of high-density, small electrodes reported a low acute yield [42]. This could be explained by the fact that small electrodes typically have recording sites of smaller surface area, which can make it difficult to achieve the low impedances often needed for single unit recording. Increasing the surface area is one possible solution, which has unknown effects on the yield of small single unit spike detection [47, 48]. Even without active scar formation around the probe, biofouling of adherent proteins within the first few days of implant can cause a sharp increase in electrical impedance [55]. It is also possible for neurons to be present but quiescent due to inflammation [56], which could also lead to lower apparent recording yield.

In our own group, previous carbon fiber arrays yielded neural units on fewer than half of the electrodes on average when chronically implanted in motor cortex [46], with signals decreasing after several months despite minimal scarring [28]. In the present study, we investigated potential reasons for this low yield, and attribute it primarily to inconsistent tip exposure from manual cutting of the carbon fibers. We explored heat-based cutting approaches, and found that a novel laser cutting technique achieved consistent recording site exposure in a batch, repeatable process with minimal labor. While only increasing the surface area to 257 μm^2 , this technique resulted in electrodes of relatively small geometric volume and significantly lower average impedance than the conventional scissor cut electrodes. Furthermore, laser cut electrodes enabled high unit yield in both acute and chronic recordings in the rat motor cortex. Additionally, this study found that longer-lived electroplated materials, such as platinum

iridium, or carbon-only surface modifications, such as oxygen plasma surface roughening, perform well on laser cut electrodes in accelerated soak tests as compared to a conventional electrodeposited polymer coating.

2. Methods

2.1. Experimental design

In this work, we first explored fabrication methods to expose the recording surface of carbon fiber electrodes. The most suitable exposure method was characterized by *in vivo* recording yield in acute and chronic settings. The chronic recording yield was compared to our previous scissor cut carbon fiber electrode from Patel *et al* 2016 [28]. Secondly, we tested our standard electrode coating material for degradation and explored alternative coatings and treatments for the recording site.

2.2. Carbon fiber array fabrication

The electrodes in this study were composed of electrically conductive strands of carbon fiber (T-650/35 3 K, Cytec Thornel, Woodland Park, NJ). The 6.8 μm diameter carbon fibers were attached to printed circuit boards (PCBs) designed to facilitate electrical recordings. Electrode fabrication followed the steps previously described in Patel *et al* 2015 and 2016 [28, 46]. In brief, individual, uninsulated carbon fibers were manually placed and electrically connected to the bond pad or exposed gold trace of the PCB using conductive silver epoxy (H20E, Epoxy Technology Inc., Billerica, MA). After baking, the junction was covered with an insulating epoxy (353ND-T, Epoxy Technology Inc., Billerica, MA). The entire device was insulated with approximately 800 μm of parylene-c using 2 g of precursor (PDS2035CR, Specialty Coatings Systems, Indianapolis, IN). Electrode tip fabrication continued in Section 2.3.

Several array designs were used in this study, all previously described in Patel *et al* 2015 and 2016 [28, 46]. The first array, a large PCB design called a Wide Board (WB), contained up to 8 fibers per array and was used in the accelerated soak tests for ease of handling (figure S4) [28]. The second array, a smaller PCB called a ZIF array, contained up to 8 fibers per array and was developed for *in vivo* neural recordings using the Tucker-Davis Technologies ZIF headstage (Tucker-Davis Technologies, Alachua, FL) (figure S4) [46]. In some cases, the ZIF array was exchanged for a third array, a preliminary device containing up to 16 fibers that uses a permanent shuttle, similar to that shown in Patel *et al* 2015, to avoid PEG application during insertion.

2.3. Carbon fiber electrode tip preparation

After parylene-c insulation, fibers were manually cut to the final desired length using stainless steel microsurgical scissors (15002-08, Fine Science Tools,

Foster City, CA) or ceramic microsurgical scissors (15750-11, Fine Science Tools, Foster City, CA) under a stereoscope equipped with a reticle. Carbon fibers were cut to 500 μm for SEM imaging, 2 mm for *in vivo* implantation, and 5 mm for accelerated soak testing. Fibers were laser cut using a 532nm Nd:YAG pulsed laser (LCS-1, New Wave Research, Fremont, CA; 5 mJ/pulse, 5 ns pulse duration) at a power of 900mW and intensity of 100% in combination with a Karl Suss probe station (LC3, SUSS MicroTec, Garching, Germany) for optical alignment. The device was secured to a glass slide and the tip of each fiber was aligned within the 22 μm by 75 μm window of the laser. The laser was pulsed an average of 3 times to completely remove the roughly 75 μm length of the fiber that was within the window.

2.4. Electrochemical deposition of coatings and oxygen plasma treatment

The exposed site on laser cut fibers was electrodeposited with a solution of 0.01M 3,4-ethylenedioxythiophene (483028, Sigma-Aldrich, St. Louis, MO) and 0.1 M sodium p-toluenesulfonate (152536, Sigma-Aldrich, St. Louis, MO) by applying 600 pA/channel for 600 s to form a layer of poly(3,4-ethylene dioxythiophene):sodium p-toluenesulfonate (PEDOT:pTS) [28, 45, 46, 57]. PEDOT:pTS was deposited on scissor cut fibers by applying 100 pA/channel, as previously done in our carbon fiber work [28, 46]. High-surface area electrodeposited platinum-iridium (PtIr) coating (Platinum Group Coatings, Pasadena, CA) was deposited onto the exposed section of the laser cut carbon fibers using a process described previously by Petrossians *et al* 2011 [58]. The presence of PtIr after electrodeposition was confirmed by an increase in current drawn during cyclic voltammetry (CV) and a decrease in 1 kHz impedance measured by electrochemical impedance spectroscopy (EIS). Fibers were treated with oxygen plasma (O_2P) in the Glen 1000P Plasma Cleaner (pressure 200 mT, power 300 W, time 120 s, oxygen flow rate 60 sccm, and argon flow rate 7 sccm) by placing the arrays on a floating tray beneath active plasma bombardment.

2.5. Electrochemical impedance spectroscopy (EIS) and cyclic voltammetry (CV)

To characterize fabrication and deposition steps, three-electrode EIS measurements were taken with a PGSTAT12 Autolab potentiostat (Metrohm/Eco Chemie, Utrecht, Netherlands) controlled by the vendor supplied NOVA software. Fibers were submerged by 1 mm in 1x phosphate buffered saline (PBS, BP3994, Fisher, Waltham, MA). An Ag|AgCl electrode (RE-5B, BASi, West Lafayette, MA) served as a reference electrode and a stainless steel rod was selected as the counter electrode to better match the stainless steel bone screw counter electrode used *in vivo* [28, 46]. EIS measurements were obtained by

applying a $10 \mu V_{RMS}$ signal from 10 Hz to 31 kHz. CV measurements were obtained by sweeping three times between 0.8 V to -0.6 V and 0.8 V at a scan rate of 1 Vs^{-1} . Prior to EIS measurements, PtIr coated electrodes were conditioned using a scan rate of 0.5 Vs^{-1} with step potential of -0.01 V for a total of 13 sweeps in order to remove any extraneous debris [59]. EIS and CV measurements were analyzed using custom Matlab (Mathworks, Natick, MA) scripts. Fibers were cleaned in deionized water after EIS measurements.

2.6. Scanning electron microscopy (SEM) and energy-dispersive x-ray spectroscopy (EDS)

SEM images were collected of carbon fibers at various stages of the fabrication and experimental process. All images were collected in either the Nova Nanolab 200 DualBeam SEM (FEI, Hillsboro, OR) or the TESCAN Rise SEM (Tescan Orsay Holding, Brno–Kohoutovice, Czech Republic), using 2 kV or 16 kV accelerating voltage and 0.21 nA or 165.90 μA current, respectively. SEM analysis of different fiber tip cutting methods used ZIF arrays with 500 μm length fibers mounted on standard SEM pin stub mounts (16111, Ted Pella, Redding, CA) using double sided carbon tape (16073, Ted Pella, Redding, CA). The mounted fibers were then sputtered with gold for one to two minutes (11429, Structure Probe, Inc. West Chester, PA) and imaged on the Nova Nanolab SEM at either a 45° or 60° tilt with a 12 kx magnification using the Everhart-Thornley detector. Similarly, plating evaluation was performed with ZIF arrays prepared with 2 mm fiber lengths, coated with PEDOT:pTS or treated with O_2P , sputtered with gold for two minutes, and imaged in the Nova Nanolab SEM using the same settings. The PtIr-coated fibers of 2 mm length were prepared on ZIF arrays and imaged in the the Tescan Rise SEM using a low vacuum acquisition mode, allowing for imaging without gold coating. The fibers were imaged using the low vacuum secondary electron Tescan detector at a 20° tilt with a magnification of 8 kx. Fibers were imaged after the accelerated soak test in the Tescan Rise using low vacuum acquisition mode. Charging was reduced by touching the 5 mm long fibers to a piece of silicon wafer during imaging. SEM images of explanted fibers were collected in the Tescan Rise using low vacuum acquisition mode after 1 min and 20 s of gold sputtering. EDS analysis was performed using the Tescan Rise to chemically characterize the PEDOT:pTS coated carbon fibers before and after the accelerated soak test. The analysis was done at 10 kV at a working distance of 15 mm, acquiring both an EDS map and spectra signals of the coated surface.

2.7. Accelerated soak test setup

Similar to our previously documented accelerated soak test assembly in Patel *et al* 2016 [28], the soak test was conducted on 8-fiber WBs in a water bath (FSGPD05, Thermo Fisher, Hampton, NH) set to

50° C . Four WBs were secured to the underside of the lid of a glass jar using a 16-pin DIP socket secured with epoxy (353ND-T, Epoxy Technology Inc., Billerica, MA). The lids were fastened to the soak test jars, which were filled with 1x PBS solution (BP3994, Fisher, Waltham, MA) to a level such that the tips of the fibers were submerged by several millimeters into the PBS. Three jars were used to hold a total of 12 WBs, three from each of the following categories: laser cut PEDOT:pTS-coated fibers, laser cut PtIr-coated fibers, laser cut O_2P -etched fibers, and uninsulated bare fibers that served as the control. The control boards received the same fabrication steps prior to parylene-c coating. They were used to indicate any degradation of the PCB itself. The WBs were randomly distributed between the jars at the beginning of the experiment. At the time of measurement, the jars were removed from the soak test bath and each WB was rinsed in deionized water. Normal EIS measurements were then conducted for each WB. Following measurements, the jars were then rinsed, filled with fresh PBS, and returned to the water bath with the WBs secured. The position of the jars within the water bath was shifted following each measurement to account for any heating irregularities in the water bath.

Similar to Patel *et al* 2016 [28], and the works by Green *et al* [57] and Hukins *et al* [60], the simulated aging time of the heated fibers can be determined by the equation

$$t_{37} = t_T \times Q10^{(T-37)/10}$$

in which t_{37} is the simulated aging time at 37° C , t_T is the amount of real time that the samples have been kept in heat at temperature T, and Q10 is an aging factor that is equal to 2, according to ASTM guidelines for polymer aging [61]. Calculating the simulated time for $t_T = 1$ and $T = 50^\circ \text{ C}$ results in $t_{37} = 2.46$. This value of 2.46 is the acceleration factor and all real time measurements are scaled by this amount to obtain the simulated time.

2.8. Electrode preparation for surgical implantation

EIS measurements were collected and electro-physiology ground and reference wires (AGT05100, World Precision Instruments, Sarasota, FL) were soldered to the ZIF PCB, each with roughly 5 mm of exposed contact at the end. Fibers attached to ZIF arrays were rinsed with deionized water prior to prepping with 2050MW poly(ethylene glycol) (PEG, 295906, Sigma Aldrich, St. Louis, MO), a non-toxic material that temporarily stiffens the fibers in order to increase insertion depth without fiber buckling, as explored in Patel *et al* 2015. Briefly, the row of 8 fibers were gently rested on an aluminum foil surface lightly coated with mineral oil (M8410, Sigma Aldrich, St. Louis, MO). A coil of wire was wrapped around a soldering iron set to 500° F and used to pick up a single

flake of 2050MW PEG. Once melted, the droplet of liquid PEG was brushed along the length of the fibers, leaving the very tip of fibers exposed. The fibers easily released from the oiled surface once the PEG cooled.

2.9. Surgical procedures for implantation of carbon fibers

All animal procedures were approved by the University of Michigan Institutional Animal Care and Use Committee.

Surgical procedures of carbon fiber arrays used adult male Long Evans rats weighing 400–500 g. Vitals were monitored during surgery using a pulse-oximeter and rectal temperature probe. Animal preparation for carbon fiber insertion followed the procedure described in Patel *et al* 2015. In brief, once the skull surface was cleaned, a burr bit (19008–07, Fine Science Tools, Foster City, CA) was used to drill holes for the bone screws (19010-00, Fine Science Tools, Foster City, CA). Acute rats received one bone screw near the posterior edge of the skull, while chronic rats had seven holes placed around the periphery of the skull. Next, a 2.5 mm by 2.5 mm craniotomy was made over the right hemisphere's motor cortex according to a reference atlas [62]. Following dura resection, the PEG coated fibers on the ZIF array were brought near the surface of the brain with fibers aligned along the anterior-posterior axis. The exposed fibers were driven into the brain manually using a stereotactic manipulator until the PEG coated portion reached the surface of the brain, at which point a small amount of Lactated Ringer's (2B2324, Baxter, Deerfield, IL) was applied to the craniotomy via syringe to dissolve the PEG nearest to the brain. The fibers were then manually driven in further until the final target depth of 1.2 mm to layer V was reached [63] and all remaining PEG was dissolved. Acute non-survival surgeries were performed on $N = 3$ animals, with one animal receiving a ZIF array and the other two each receiving a permanent shuttle array.

For chronic animals, silicone (3–4680, Dow Corning, Midland, MI) was added via syringe to the craniotomy to cover fiber length above the brain surface to the junction with the PCB. Ground and reference wires were then wound around the ground bone screw. Dental acrylic was applied to the skull, bone screws, and PCB to form a headcap. The skin flaps were sutured together at the anterior and posterior ends of the headcap and triple antibiotic ointment was liberally applied. Animals were then removed from the stereotax and allowed to recover on a heated pad placed under their cage. Chronic survival surgeries were performed on $N = 4$ animals, with two animals receiving ZIF arrays and two receiving permanent shuttle arrays.

2.10. Electrophysiology recordings

The collection of all electrophysiology recordings was done using a ZC16 headstage, RA16PA

pre-amplifier, and RX5 Pentusa base station (Tucker-Davis Technologies, Alachua, FL). During data acquisition, the pre-amplifier high-pass filtered at 2.2 Hz, anti-alias filtered at 7.5 kHz, and sampled at a rate of 25 kHz. Recordings done with acute implants took place while the rats were under ketamine/xylazine anesthesia, while the chronic electrophysiology measurements were collected on awake and behaving animals, as described in Patel *et al* 2015. Each recording session lasted 3 and 10 min for acute and chronic implants, respectively. This study also analyzed chronic electrophysiology recordings from $N = 6$ animals reported in Patel *et al* 2016. The neural data was collected on $N = 77$ scissor cut PEDOT:pTS coated carbon fiber electrodes mounted on ZIF arrays.

2.11. Histological analysis

Animals were transcardially perfused and brains were extracted, as detailed in Patel *et al* 2016, after 91 or 94 days of implant. Explanted headcaps were soaked in enzymatic cleaning solution (J-J2252, Enzol, Johnson & Johnson, New Brunswick, NJ) for 1.5 hours, rinsed in dionized water, and dried prior to SEM imaging. For immunohistochemical analysis, we chose six 100 μm thick slices that contained the targeted region of motor cortex where the carbon fiber electrodes were implanted. To assess neuronal health, we stained the sections to visualize all cells, neurons, astrocytes, and microglia. The slices were incubated in 4%(w/v) paraformaldehyde (P6148, Sigma Aldrich, St. Louis, MO) (pH 7.40) in 1x PBS overnight as a post-fixation step and washed in 1x PBS at room temperature for two hours the following day. We then placed the slices in a blocking solution containing StartingBlock™ (PBS) Blocking Buffer (37578, Thermo Fisher, Waltham, MA) and 1.0% Triton X-100 (T8787, Sigma Aldrich, St. Louis, MO), overnight at room temperature, followed by three washes in 1x PBS containing 0.5% Triton X-100 (0.5% PBS-T) at room temperature, one hour each. The slices were incubated in a solution containing StartingBlock™ (PBS) Blocking Buffer, 1.0% Triton X-100, and the following primary antibodies: Mouse anti-NeuN (MAB377, Millipore, Billerica, MA), Rabbit anti-GFAP (Z0334, Dako, Carpinteria, CA), and Guinea Pig anti-Iba-1 (234004, Synaptic Systems, Goettingen, Germany), for three nights at 4 °C in a covered chamber. The slices were then triple rinsed with 0.5% PBS-T, with each wash lasting one hour. The slices were then incubated in a solution containing StartingBlock™ (PBS) Blocking Buffer, 1.0% Triton X-100, and the following secondary antibodies: Donkey anti-Mouse IgG Alexa Fluor 647 (715-605-150, Jackson, West Grove, PA), Donkey anti-Rabbit IgG Alexa Fluor 546 (A10040, Life Technologies, Waltham, MA), Donkey anti-Guinea Pig Alexa Fluor 488 (706-545-148, Jackson, West Grove, PA), and DAPI (D1306, Invitrogen, Grand Island, NY), for two nights at 4 °C in a

covered chamber. All primary and secondary antibodies were used at a 1:250 dilution. The slices were rinsed twice in 0.5% PBS-T, each wash one hour long, followed by a final overnight wash in 1x PBS. The slices were then cover slipped with VECTASHIELD Antifade Mounting Medium (H-1000, Vector Laboratories, Burlingame, CA) and left to dry overnight to prepare for imaging with a laser scanning confocal microscope.

Imaging was performed on a Zeiss LSM 780 Confocal Microscope using a C-Apochromatic 10x/0.45W M27 water immersion objective. A 15x15 tile, 75 μm z-stack was acquired to visualize all four stains on the whole slice. Track 1 scanned with the 405 laser, track 2 scanned with the 488 and the 633 lasers, and track 3 scanned with the 543 laser. All laser intensities were adjusted manually to prevent pixel saturation and ranged from 1.2-35% laser power. The gain and contrast were altered during image processing in FIJI.

2.12. Neural data analysis

We used two methods of electrophysiology data analysis, one to spike sort in a semi-automated fashion and another to detect bipolar waveforms at set thresholds. Analysis was performed on chronic data collected 7 days after implant once recordings were believed to stabilize [64], and on day 63 or 64 after implant. Prior to analysis, chronic data was cleaned by removing time snippets containing headstage or movement artifacts. Spike sorting was conducted in Offline Sorter (OFS, Plexon, Dallas, TX) on 180 s of data common average referenced between intact fibers within each animal [29]. We made sure that common average referencing did not introduce false waveforms into datasets with small n by invalidating artifacts that appeared across all channels. For each recording session, channels were high-pass filtered (250 Hz corner, 4th order Butterworth) and waveforms were detected at a $-3.5 \times \text{RMS}$ threshold. Cluster centers were then identified in principle component space using a K-means sorting method and obvious noise clusters were invalidated [65], as determined by a trained operator. Remaining waveforms were then clustered using an automated mixture of Gaussian model (standard expectation-maximization) with fixed number of iterations, between 1 and 6 [65]. Units with similar amplitude and waveform shape were combined. For each sorted unit, we collected the average peak-to-peak waveform amplitude. Carbon fiber electrodes with discernible units following this method of analysis were considered viable in the recording yield calculation and were analyzed further using the bipolar detection method described below.

The second method of neural data analysis identified bipolar waveforms of un-referenced data at a set voltage cut off on viable electrodes identified using

the previous cluster sorting method. After high-pass filtering, 50 s of clean data from each intact fiber was thresholded at $-45 \mu\text{V}$. The fibers that did not detect identifiable units in the OFS technique were not included in this analysis. The resultant waveforms from the threshold crossing were then determined to be bipolar using several constraints: the minimum peak must occur within the 0.33 ms of the negative threshold crossing, followed by the maximum peak within 0.53 ms, and the rising edge following the minimum peak must pass a $+40 \mu\text{V}$ threshold within 0.49 ms of the negative threshold crossing. The peak-to-peak voltage amplitudes of the bipolar waveforms were then grouped by size and the percentage of channels that detected waveforms of set amplitude were determined. A minimum of 10 waveforms within 50 s were needed in order for the channel to be counted at that threshold.

2.13. Statistical analysis

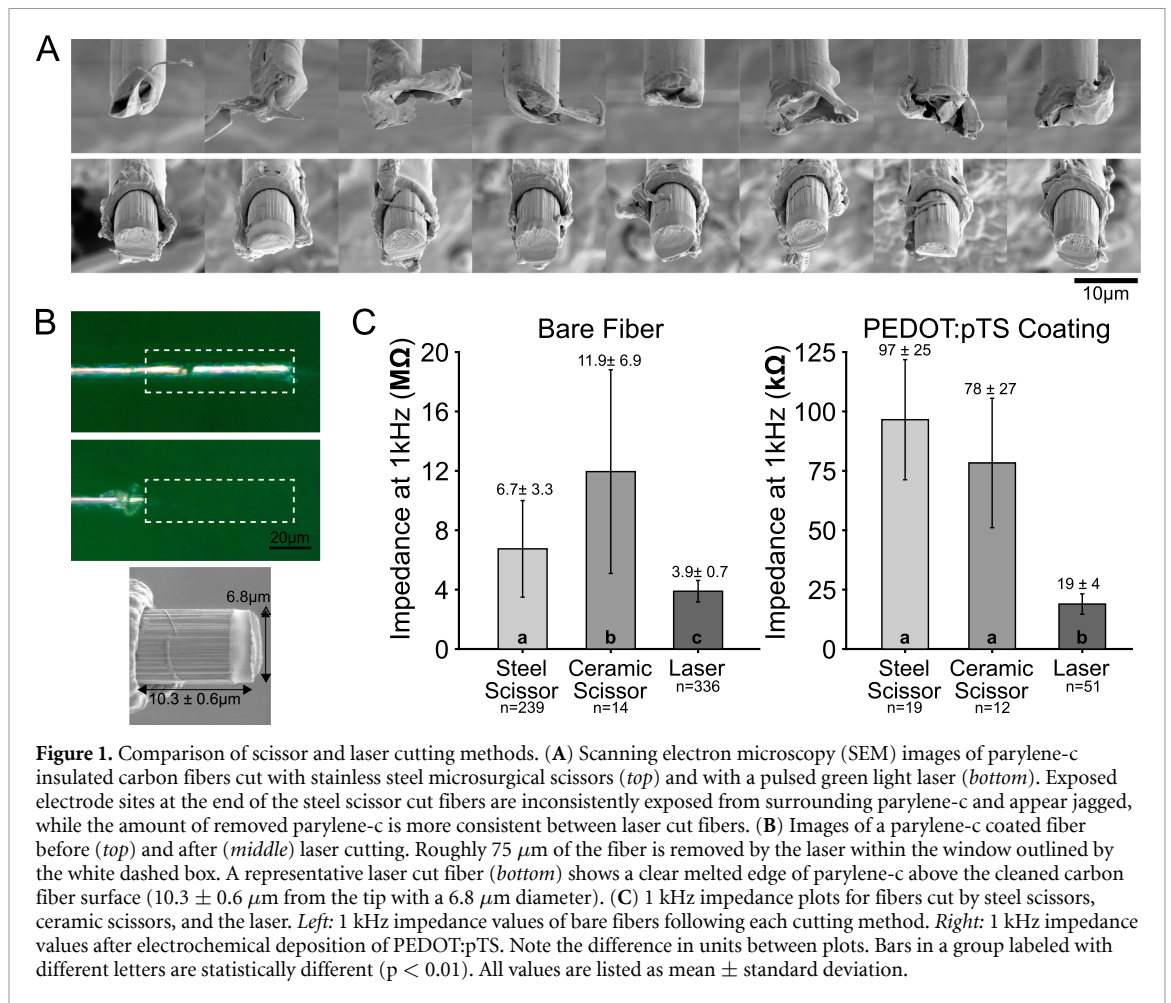
One kilohertz impedance magnitudes were compared between cut and coating groups using a Welch's two-sample, one-tailed t-test using 0.01 alpha level. The increase in 1 kHz impedance during the accelerated soak test was compared between groups using a Welch's two-sample, one-tailed t-test using a 0.01 p-value. All calculations were carried out in MATLAB (Mathworks, Natick, MA).

3. Results

3.1. Improved electrode tip fabrication with laser cutting

The basis for this work was to investigate the underlying limitation of previous chronic implants of carbon fiber arrays in which a low percentage of implanted carbon fiber electrodes was able to record neural units, despite immediate healthy neuronal tissue adjacent to recording sites at time of euthanasia. Firstly, we hypothesized that the problem could lay in our fabrication process, and began by evaluating the method used to create the recording site at the carbon fiber tip. Specifically, in our previous studies, carbon fibers were cut using microsurgical stainless steel scissors immediately after insulating the device with parylene-c as previously explained in Patel *et al* 2015 [46].

We evaluated this approach using SEM images of carbon fiber tips after being cut with steel scissors ($N = 8$ fibers). As shown in figure 1A, steel scissor cutting often caused the parylene-c to fold over the electrode recording site, partially or completely enclosing the recording active surface. Out of eight fibers viewed, the over folding was qualitatively observed in seven cases. Fibers also exhibited a jagged and irregular carbon surface, often depressed from the parylene-c edge. Seeking more consistency, we also tried cutting fibers with scissors of a harder ceramic material. However, these scissors had similar difficulties when



qualitatively evaluated (figure S1). While we achieved a near perfect cut using a focused ion beam with gallium ions, this approach required tens of minutes per fiber on a high cost tool and was not further pursued (figure S1).

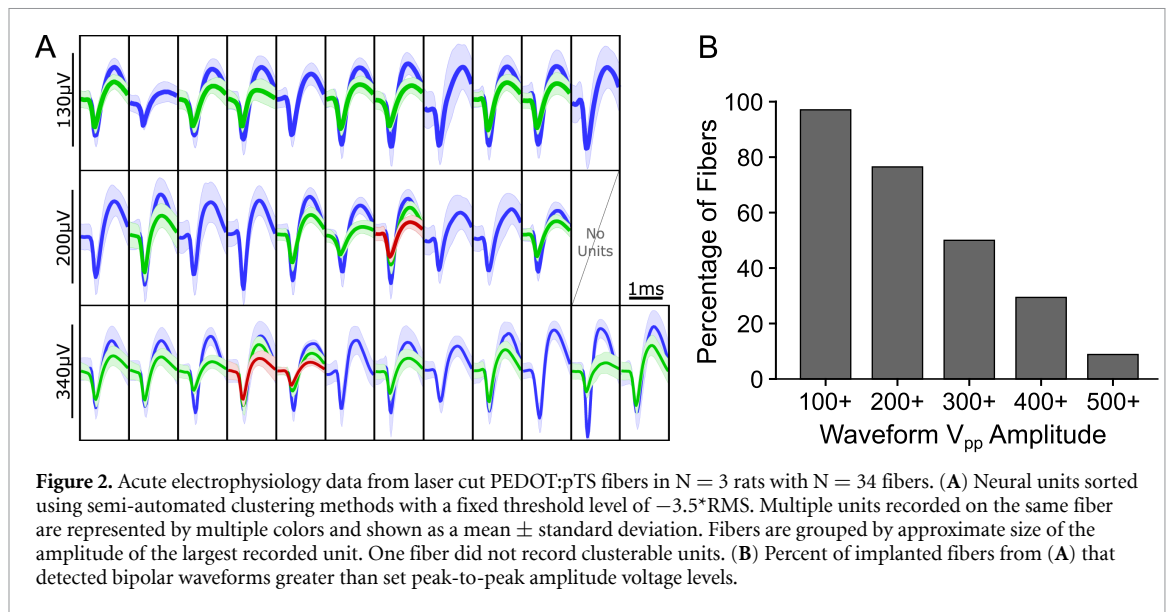
We then sought a heat based cutting method that would allow for rapid cutting of many fibers with high fiber-to-fiber consistency and controllable amounts of parylene-c removal. We tried multiple laser-based approaches and chose a 532 nm Nd:YAG pulsed laser to ablate sections of parylene-c along the carbon length to create electrode sites. By increasing the laser power to 900mW, it was possible to cleanly cut the carbon fiber tip with several pulses (3 pulses, N = 184 fibers). As qualitatively shown in figure 1A, this method reliably revealed more surface area at the electrode tip compared to mechanical cutting techniques. Parylene-c was burned back an average of $10.3 \pm 0.6 \mu\text{m}$ from the tip (N = 8 fibers), for an average surface area of $257 \pm 0.6 \mu\text{m}^2$, assuming a $6.8 \mu\text{m}$ diameter (figure 1B). Predictably, this had large implications for electrode impedance. Figure 1C shows the 1 kHz impedance for bare fibers cut by both scissor methods and the laser. Impedance is significantly different between traditional steel scissor cut fibers (N = 239 fibers) and laser cut fibers (N = 336 fibers), with impedance values decreasing from $6.7 \text{ M}\Omega$ to $3.9 \text{ M}\Omega$ ($p < 0.01$). The standard deviation of laser cut fibers

is also lower than steel cut fibers, $720 \text{ k}\Omega$ and $3.3 \text{ M}\Omega$, respectively. Unexpectedly, cutting with ceramic scissors (N = 14 fibers) resulted in a high average impedance of $11.9 \pm 6.9 \text{ M}\Omega$, significantly different than steel scissor ($p < 0.05$) and laser cut fibers ($p < 0.01$).

To transform these fibers into functional recording sites, we applied an additional conductive coating of PEDOT:pTS that has been used in our previous carbon fiber work [28, 45, 46]. As expected, the PEDOT:pTS coating lowered the 1 kHz impedance dramatically in all cases (figure 1C). The resulting 1 kHz impedance of cut fibers was $97 \pm 25 \text{ k}\Omega$ for steel scissors (N = 19 fibers), $78 \pm 27 \text{ k}\Omega$ for ceramic scissors (N = 12 fibers), and $19 \pm 4 \text{ k}\Omega$ for the laser (N = 51 fibers). This difference was significant between steel scissors and laser ($p < 0.001$), ceramic scissors and laser ($p < 0.001$), but not between the two scissor types ($p > 0.05$). All results hereafter referencing scissor cutting utilize steel scissors. Given the visual consistency of the laser cut fibers and the reduced impedance value and variability between laser cut fibers, we continued our testing with laser cut fibers *in vivo*.

3.2. Recording yield increase for laser cut fibers coated with PEDOT:pTS

Given the extremely small cross section of cellular-scale electrodes, including carbon fibers, and the very high density of neurons in cortex, it has been unclear



why the unit yield has not been near 100%, at least in a short chronic setting before any material failures. While this could be related to insertion damage, silent neurons, or anesthesia, we evaluated here whether these lower impedance and more consistent electrode tips could enable the acute recording of neural activity on every channel.

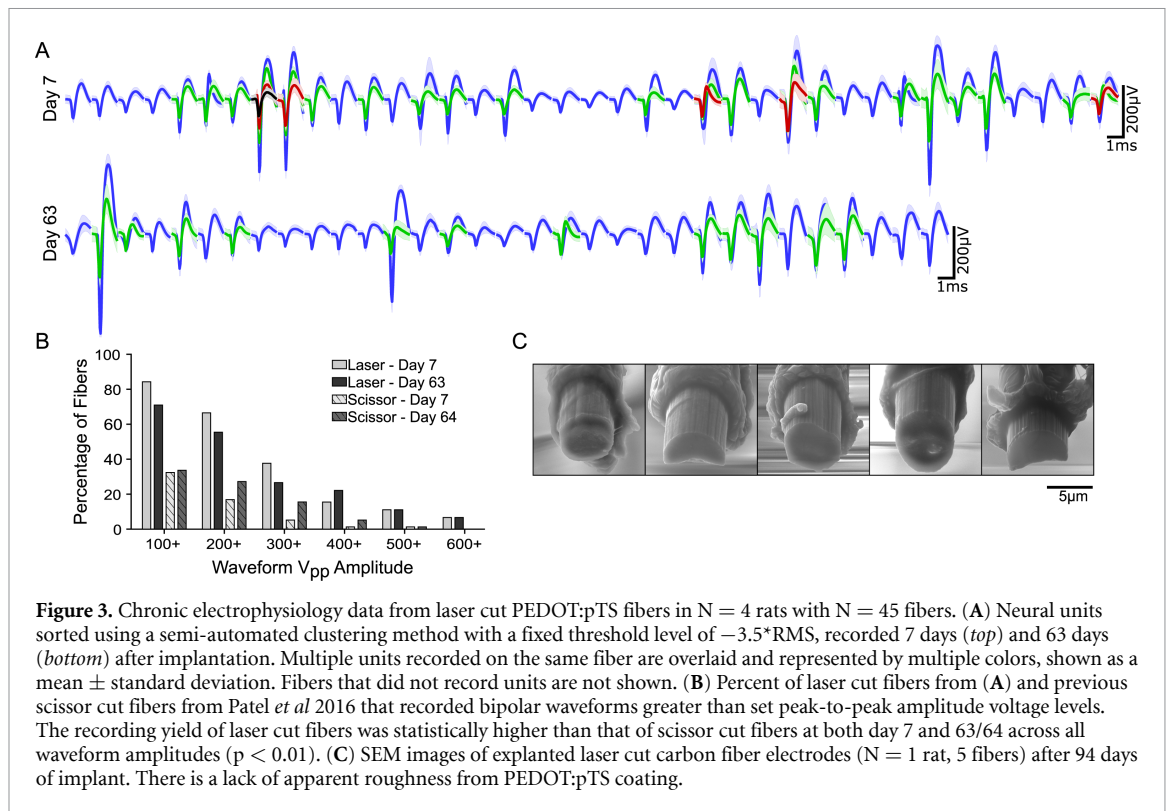
We tested this by acutely implanting 34 laser cut PEDOT:pTS-coated fibers into the layer V of the motor cortex at a 1.2 mm depth in three rats. To quantify these waveforms in an objective manner, we took several different approaches. First, we evaluated the number of clusterable units detected on each electrode using a semi-automated sorting method. With a set threshold of $-3.5 \times \text{RMS}$, we used principal component analysis and both K-means and a mixture of Gaussians sorting methods on this data. The resulting spike panel is shown in figure 2A. While many of these units encompassed waveforms across a range of amplitudes, 97% of PEDOT:pTS-coated laser cut electrodes recorded clusterable units in this acute setting. We recorded a total of 57 units across the 34 electrodes, averaging 1.7 units/electrode, with an average unit amplitude of $150.6 \pm 80.2 \mu\text{V}_{pp}$ (mean \pm sd).

Second, we broadly evaluated the range of bipolar waveforms amplitudes that the electrodes could detect from any nearby neural activity. Based on the noise level of our setup, we set a threshold at $-45 \mu\text{V}$ and checked for clear bipolar 1 ms long waveforms. Under ketamine, bipolar waveforms of at least $85 \mu\text{V}_{pp}$ amplitude appeared on 97% of all carbon fiber electrodes, consistent with healthy firing neurons within recording range of almost every electrode tip. A histogram of the percent of electrodes with recorded waveforms larger than increasing amplitude values is shown in figure 2B. A total of 97% of electrodes recorded waveforms of amplitudes larger than $100 \mu\text{V}$, 76% had waveforms greater than $200 \mu\text{V}$, 50%

had waveforms greater than $300 \mu\text{V}$, 29% of electrodes had waveforms greater than $400 \mu\text{V}$, and 9% had waveforms greater than $500 \mu\text{V}$. We found from these acute tests that PEDOT:pTS-coated laser cut carbon fiber electrodes have a high recording yield of clusterable single units and record high amplitude bipolar waveforms.

The results from our acute tests prompted us to further evaluate the long-term effectiveness of laser cut PEDOT:pTS carbon fibers. We therefore chronically implanted 4 rats with a total of 45 laser cut carbon fibers and compared the chronically recorded neural activity from laser cut fibers to our previous work using scissor cut fibers at days 7 and 63/64. Within the first week of implant, biofouling and the associated impedance increase [55], tissue swelling, and fluid build up cause low and inconsistent recording yields [64]. We chose to examine day 7 when biofouling and tissue recovery have stabilized and PEDOT:pTS aging is likely not to have occurred by that point. After two months of implant, however, any mechanical failures or PEDOT:pTS degradation may have occurred.

Chronically recorded neural activity is shown in figure 3. We analyzed the data using the same methodology as the acute recordings. A semi-automated spike sorting showed a 84% recording yield of laser cut PEDOT:pTS coated fibers on day 7 ($N = 45$ fibers) with an average amplitude of $172 \pm 96 \mu\text{V}$ on day 7 (figure 3A). Viewing 50 s of artifact-free data, the same $-45 \mu\text{V}$ and $+40 \mu\text{V}$ thresholds with minimum peak constraint were applied (figure 3B). Similar to the acute data, 84% of electrodes had units larger than $100 \mu\text{V}$, 67% of electrodes had units larger than $200 \mu\text{V}$, 38% of electrodes had units larger than $300 \mu\text{V}$, 16% of electrodes had units larger than $400 \mu\text{V}$, 11% of electrodes had units larger than $500 \mu\text{V}$, and 7% of electrodes had units larger than $600 \mu\text{V}$. We applied these same semi-automated sorting techniques to



reanalyze the day 7 neural data collected on steel scissor cut fibers from Patel *et al* 2016 and found a 180% increase in recording yield from this previous study [28]. For the same waveform amplitudes values, the recording yield of implanted scissor cut PEDOT:pTS coated fibers on day 7 was 32%, 17%, 5%, 1%, 1%, and 0% (N = 77 fibers).

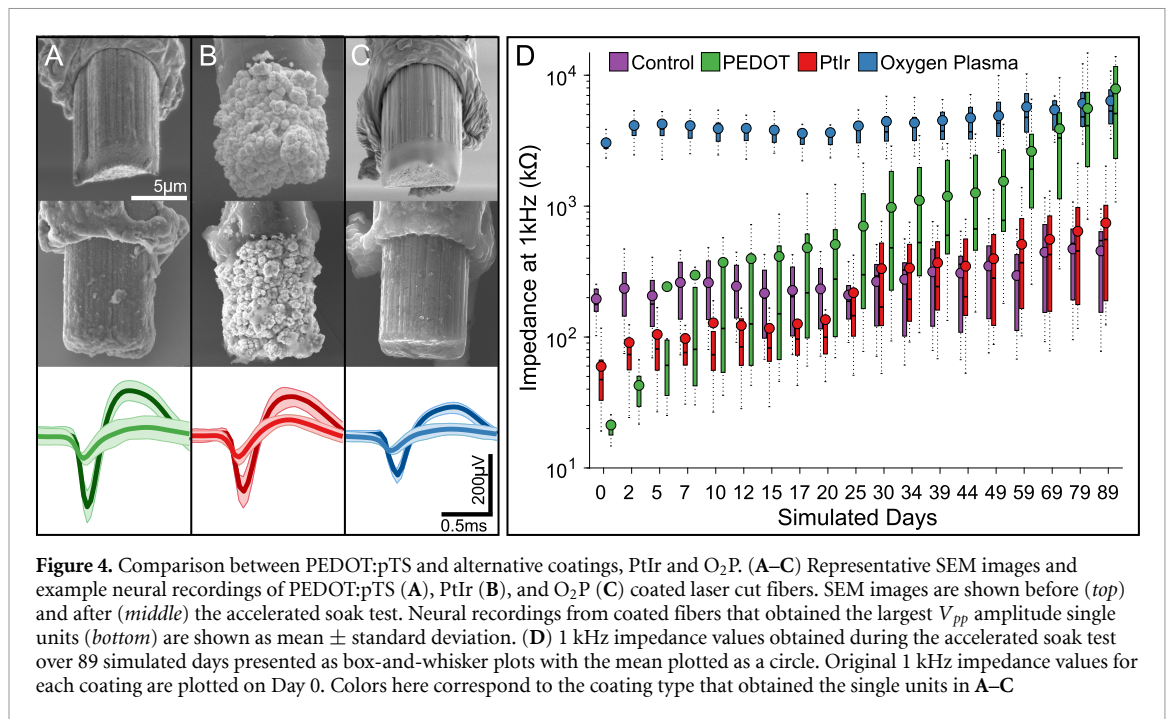
By day 63, the recording yield of laser cut fibers remained high at 71% (N = 45 fibers), shown in figure 3. The average amplitude of units on day 63 was observed as $171 \pm 109 \mu\text{V}$ (figure 3A). Analyzed in the same manner as previous data, 71% of electrodes had units larger than $100 \mu\text{V}$, 56% of electrodes had units larger than $200 \mu\text{V}$, 27% of electrodes had units larger than $300 \mu\text{V}$, 22% of electrodes had units larger than $400 \mu\text{V}$, 11% of electrodes had units larger than $500 \mu\text{V}$, and 7% of electrodes had units larger than $600 \mu\text{V}$ (figure 3B). The scissor cut recording data from Patel *et al* 2016 followed a similar pattern on day 64 as on day 7 [28]. For the same waveform amplitude values, the recording yield of implanted scissor cut fibers on day 64 was 34%, 27%, 16%, 5%, 1%, and 0%. The recording yield of laser cut fibers was statistically higher than that of scissor cut fibers at both day 7 and 63/64 across all waveform amplitudes ($p < 0.01$). This suggests that not only do laser cut fibers have higher chronic recording yield, but also larger amplitude units. After 3 months, two of the four rats exhibited complete failure due to grounding or breakage, while the remaining two rats maintained a recording yield of 79% (N = 24 fibers).

We performed histology on tissue slices several hundred microns dorsal from the recording tip on

two animals with laser cut electrodes. Arrays were implanted roughly 2 mm lateral from midline in the anterior half of the brain and a representative image containing the region of implant is shown in figure S2. Similar to Patel *et al* 2016, it was difficult to identify holes in the tissue corresponding to the location of implanted fibers, however the similarity between hemispheres points to minimal damage from the $8 \mu\text{m}$ carbon fiber electrodes. Images of explanted fibers for one rat are shown in figure 3C. Fibers appear intact without any attached biological debris, which may be due to enzymatic cleaning after explant, but do not appear to have obvious PEDOT:pTS coating.

3.3. Impedance increase associated with PEDOT:pTS degradation

Laser cut carbon fibers coated with PEDOT:pTS facilitated promising neural recording results and increased the overall recording yield of our electrode arrays to 97% and 84% in acute and 7-day chronic time frames. However, within weeks of chronic implant, the laser cut PEDOT:pTS electrodes exhibited a decrease in recording yield and an increase in 1 kHz impedance, similar to that of our previous scissor cut PEDOT:pTS electrodes [28]. The 1 kHz impedance of the chronically implanted laser cut electrodes began at $107 \pm 139 \text{ k}\Omega$ on day 1 and increased to $1.2 \pm 1.0 \text{ M}\Omega$ on day 7, $2.5 \pm 2.0 \text{ M}\Omega$ on day 63, and $2.7 \pm 1.8 \text{ M}\Omega$ on day 91/94 (N = 45 fibers, mean \pm sd). This increase of roughly $2.6 \text{ M}\Omega$ was similar to that of previous chronic scissor cut PEDOT:pTS experiments. The chronic 1 kHz impedance values



from Patel *et al* 2016 at the same time points were $670.8 \text{ s} \pm 540.7 \text{ k}\Omega$, $1.7 \pm 1.3 \text{ M}\Omega$, $2.8 \pm 1.7 \text{ M}\Omega$, and $2.9 \pm 1.8 \text{ M}\Omega$ ($N = 77$ fibers, mean \pm sd). While recording systems with high input impedance amplifiers, as are often used in neuroscience research, can partially mitigate the noise generated by the high-impedance electrodes, it may be critical for other applications, such as multi-year implantable medical devices, that lower 1 kHz electrode impedance be maintained.

It was unclear, however, if the increase in impedance *in vivo* was driven by PEDOT:pTS degradation, biofouling, or some other factor. Characterizing the electrode coating in an accelerated soak test removes the complications of biofouling and tissue thermal noise, allowing for a direct comparison of long-term impedance changes between recording site treatments. Therefore, we submerged the PEDOT:pTS-coated fibers in PBS solution heated to 50°C for 36 days, equivalent to a simulated 88.64 days [28]. Similar to our previous work, the impedance of PEDOT:pTS laser cut fibers increased dramatically over the 36 day accelerated soak test, seen in figure 4D. Before testing, the average PEDOT:pTS 1 kHz impedance was $21 \pm 5 \text{ k}\Omega$, as expected (figure 4D day 0, $N = 23$ fibers). SEM images of PEDOT:pTS coated fibers immediately after electrodeposition appear characteristically roughened by the thin layer of PEDOT:pTS coating (figure 4A, top row). After approximately 7 simulated days in the accelerated soak test, the impedance rose by 1300% to $297.4 \pm 459 \text{ k}\Omega$ ($N = 23$ fibers). By the end of the soak test, the average PEDOT:pTS 1 kHz impedance was $7.9 \pm 7.6 \text{ M}\Omega$ ($N = 21$ fibers), indicating substantial PEDOT:pTS loss or degradation. Figure 4D shows this increasing trend

in the 1 kHz impedance values of the PEDOT:pTS coated fibers. SEM images collected after the accelerated soak test showed a smoothed carbon fiber surface with little to no roughness from PEDOT:pTS coating and some visible dried saline debris (figure 4A, middle row). We characterized the integrity of the PEDOT:pTS coating after the soak test using energy dispersive x-ray spectroscopy (EDS). We observed a decrease in sulfur composition from 6.6% ($N = 2$ fibers) to $1.6\% \pm 0.75\%$ (figure S3, $N = 20$ fibers).

The observed impedance increase and apparent PEDOT:pTS degradation led us to explore other potential coating options in a preliminary study. We explored both platinum iridium (PtIr) and patterning of the carbon itself with oxygen plasma. PtIr is commonly used in long-term medical devices [66] and has been shown to be an effective coating of microelectrodes for neural recording [59]. Coating carbon fibers with approximately $2 \mu\text{m}$ of PtIr (figure 4B, figure S5) resulted in a 1 kHz impedance of $71.0 \pm 82.5 \text{ k}\Omega$ (figure 4D day 0, $N = 137$ fibers). We attribute the decreased impedance to the rough surface of the PtIr and the electroactive nature of the PtIr alloy [67]. We also evaluated carbon-only uncoated laser cut tips that had been roughened with oxygen plasma (O₂P), seen in figure 4C. The O₂P treatment pits the surface of the carbon, reducing the 1 kHz impedance to $3.0 \pm 1.0 \text{ M}\Omega$ (figure 4D day 0, $N = 119$ fibers), within range capable of recording neural activity using a high impedance amplifier.

We qualitatively checked that the coatings thoroughly covered the surface of the carbon recording site without increasing the volume of the electrode. The SEMs showed that both PEDOT:pTS and PtIr

Table 1. Accelerated soak test trends. Summary of linear regression coefficients, standard error, p-value, and coefficient of determination for the mean 1 kHz impedance values for each coating type during the accelerated soak test over 89 simulated days.

Coating	Slope (k Ω /Day)	SE	p-value	R ²
PEDOT:pTS	71.5	7.6	3.7 ⁻⁸	0.8390
PtIr	7.7	0.3	2.0 ⁻¹⁵	0.9773
O ₂ P	30.7	2.9	7.0 ⁻⁹	0.8675
Control	2.9	0.3	2.3 ⁻⁸	0.8482

conformally coated the recording site with some over-plating up the shank, as shown in figure 4A-B. PtIr did appear to result in a slight volumetric increase, which was deemed acceptable. As expected, the O₂P treatment smoothed the overall shape of the carbon. In a single acute test to check the viability of the coated electrodes, isolated single units were detected on both PtIr-coated and O₂P-treated fibers, seen in figure 4B-C. We used the automatic OFS sorting technique described above and determined the maximum peak-to-peak amplitude of each coating type in this single acute recording session to be 396 μ V, 324 μ V, and 233 μ V for PEDOT:pTS, PtIr, and O₂P, respectively (figure 4A-C).

To evaluate longevity, we quantitatively compared the change in 1 kHz impedance values of PtIr and O₂P fibers in an accelerated soak test against our PEDOT:pTS results (figure 4D). Control boards of uninsulated bare fibers were placed with the coated fibers in the soak test to indicate degradation of the PCB. We found that the 1 kHz impedance of PtIr fibers increased by 684 k Ω (N = 24 fibers) during the course of the soak test, a significantly lower increase than the 7.8 M Ω (N = 21 fibers) increase of PEDOT:pTS fibers (p < 0.001, figure 4D). The PtIr coating was intact on the majority of fibers after the soak test with a minimal amount of saline debris (figure 4B, middle row), but in one third of the cases the PtIr appeared partially detached (N = 8 of 24 fibers), seen in figure S5B. The O₂P fibers increased by 3.3 M Ω (N = 24 fibers, figure 4D) and showed minimal saline debris (figure 4C, middle row). Control circuit boards showed slight degradation, accounting for 260 k Ω of the overall 1 kHz impedance increase (N = 24 fibers, figure 4D). A linear regression model was fit to the daily average 1 kHz impedance values for each coating type, the slope, standard error, p-value, and correlation coefficient of which are shown in table 1. We found that the slope of the 1 kHz impedance data of PEDOT:pTS coated fibers was 9 times steeper than that of PtIr.

4. Discussion

Here, we validated a laser cutting technique that produced electrodes of approximately 257 μ m² surface area, achieving a much larger apparent neuron recording yield than our previous carbon fiber work

[28]. We believe that the increase in recording yield is in part due to more consistent exposure of carbon at the tip, a volumetrically compact geometry with increased surface area, and a reduction in 1 kHz impedance. The recording site created by laser cutting may provide a stable platform for any impedance-reducing coating or treatment and result in a high recording yield. Our results here suggest that it may be possible for low damage, cellular scale electrodes to achieve high recording yield with sufficiently reliable manufacturing and materials.

The high recording yield may be a result of the more consistent, less variable laser cut electrode site. This is supported by SEM inspection and reduced variance in impedance measurements (figure 1). The yield may also be a product of the cylindrical geometry and increased surface area of the laser cut recording site. The surface area increased to 257 μ m² from the previous 36 μ m² when the electrode shape changed to a cylinder from a disc. The large exposure of the laser cut electrode site may increase access to more neurons in the surrounding tissue in three dimensions, whereas the scissor cut electrode may be more limited to neurons beneath the disk electrode. Yet, the laser cut electrode design is still volumetrically compact, with the longest dimension extending just 10 μ m across the voltage field. This compactness may lend itself to sampling from a smaller portion of the electrical field, which may enable the recording of overall larger amplitude signals [35].

The high yield we observed may also be explained by the low 1 kHz impedance produced from the laser cut, which resulted in a larger surface area. Previous carbon fiber recording electrodes have also benefited from an increased surface area, most notably those that use fire sharpening [47, 49, 52]. In one such study, approximately 90 μ m of uninsulated fiber was exposed in order to reduce the impedance into a recording-capable range of roughly 1 M Ω without the use of additional coatings [47]. However, the relationship between impedance and yield is not well understood [68] and the large increase in impedance over the roughly two months of implant may have accounted for the small but noticeable yield decrease from 84% to 71% over two months. This may indicate that recording yield may be steadily maintained if impedance is below the input impedance of the recording system amplifier [68]. Examples of silicon electrodes without additional conductive coatings have reported negligible recording yields, showing the need for lower impedance [28, 29]. Recording from neurons smaller than pyramidal cells found in layer 5 of the cortex may require the smaller surface area, lower impedance electrodes developed in this work. While further improvements are desired in tip stability, laser cut PEDOT:pTS coated carbon fiber electrodes may already provide a good alternative to traditional silicon electrodes in terms of neuronal yield for multi-month neuroscience animal studies.

There is a large shift in electrode design specifications between short-term neuroscience experiments and long-term clinical implants. Our work points to a degradation of the polymer-based PEDOT:pTS coating when immersed in a heated saline environment, both on the benchtop and *in vivo*. This degradation was initially seen by a substantial increase in 1 kHz impedance and further confirmed by a visible lack of PEDOT:pTS coating. Additionally, we found a decrease in sulfur composition in the PEDOT:pTS coating after an accelerated soak test (figure 3), a common result of PEDOT:pSS decomposition in heated, moist environments [69]. Previous work exploring the decohesion rate of PEDOT:PSS demonstrated the highly sensitive nature of the polymer to both increased moisture content and temperature [69]. This suggests that degradation of PEDOT:pTS is driving impedance increases across weeks and months.

Degradation of the electrode material is an unacceptable failure mode in a clinical BMI. Notably, our recording system with high input impedance amplifiers was able to record units with a 3 M Ω electrode, but this is not ideal for all applications. The O₂P treatment lowers the impedance into a range suitable for our recording system, but increasing the strength of the plasma bombardment may increase surface roughness and slow the impedance increase during experimentation. The PtIr coating tested here fared much better than PEDOT:pTS in accelerated soak tests, despite the mechanical detachment of PtIr on some fibers. This PtIr coating has shown promising *in vivo* results when deposited on PtIr microwire arrays [59], indicating that increasing the surface roughness of carbon prior to PtIr electrodeposition may increase coating adherence. Similar results may also be achieved with sputtered [66] or electrodeposited iridium oxide [70, 71]. It may also be possible to maximize the highly biocompatible nature of carbon [72] and use carbon-based coatings, such as two-dimensional Ti₃C₂ MXene [73] or carbon-nanotube-doped PEDOT [74, 75]. With greater improvements in device manufacturing, carbon fibers electrodes may ultimately provide the means to create a stable, high density interface to the nervous system.

Acknowledgment

This work was financially supported by the National Institutes of Health National Institute of Neurological Disorders and Stroke (U01NS094375 and UF1NS107659), the Office of the Director National Institutes of Health (OT2OD024907), as well as the National Science Foundation (1707316, DMR-0320740, and DMR-1625671). The authors acknowledge financial support from the University of Michigan College of Engineering and technical support from the Michigan Center for Materials Characterization, specifically from Mr Bobby Kerns and Dr

Allen Hunter. The authors thank the staff at the Lurie Nanofabrication Facility for their technical support. The authors thank Dr Khalil Najafi for use of his Nd:YAG laser. The authors thank Dr Curtis Lee for his assistance in PtIr electrode coating. Authors A P and J D W have a financial interest in PtIr coatings.

Author contributions

E J W fabricated electrodes, developed cutting methods, conducted rat experiments, took SEMs, analyzed data, and wrote the manuscript. P R P developed electrode designs, PEDOT:pTS deposition technique and surgical technique, and provided experimental guidance. J E W fabricated electrodes, collected EIS data, and assisted in soak test experiments. A P developed the PtIr coating and performed electrochemical deposition of electrodes. E d V collected SEM images and conducted EDS analysis of PEDOT:pTS coating. A V-M performed histological evaluation and imaging. J M R fabricated electrodes and characterized laser specifications. All authors reviewed and modified the manuscript.

ORCID iDs

Elissa J Welle  <https://orcid.org/0000-0001-5141-7656>

Paras R Patel  <https://orcid.org/0000-0001-6146-718X>

Artin Petrossians  <https://orcid.org/0000-0003-2967-8205>

Elena della Valle  <https://orcid.org/0000-0001-8874-7982>

Dawen Cai  <https://orcid.org/0000-0003-4471-2061>

James D Weiland  <https://orcid.org/0000-0003-3453-9074>

Cynthia A Chestek  <https://orcid.org/0000-0002-9671-7051>

References

- [1] Lebedev M A and Nicolelis M A L 2017 Brain-Machine interfaces: from basic science to neuroprostheses and neurorehabilitation *Physiol. Rev.* **97** 767–837
- [2] Ajiboye A B *et al* 2017 Restoration of reaching and grasping movements through brain-controlled muscle stimulation in a person with tetraplegia: a proof-of-concept demonstration *Lancet* **389** 1821–30
- [3] Bouton C E *et al* 2016 Restoring cortical control of functional movement in a human with quadriplegia *Nature* **533** 247–50
- [4] Hotson G *et al* 2016 Individual finger control of a modular prosthetic limb using high-density electrocorticography in a human subject *J. Neural Eng.* **13** 026017
- [5] Cowley J, Resnik L, Wilken J, Walters L S and Gates D 2017 Movement quality of conventional prostheses and the DEKA arm during everyday tasks *Prosthetics Orthot. Int.* **41** 33–40
- [6] Gopura R A, Bandara D S, Kiguchi K and Mann G K 2016 Developments in hardware systems of active upper-limb exoskeleton robots: a review *Rob. Auton. Syst.* **75** 203–20

- [7] Bullard A J et al 2019 Design and testing of a 96-channel neural interface module for the networked neuroprosthesis system *Bioelectron. Med.* **5** 3
- [8] Borton D A, Yin M, Aceros J and Nurmikko A 2013 An implantable wireless neural interface for recording cortical circuit dynamics in moving primates *J. Neural Eng.* **10** 2
- [9] B Smith Crish T J, Buckett J R, Kilgore K L and Peckham P H 2005 Development of an implantable networked neuroprosthesis *2nd Int. IEEE Conf. Neural Eng.* pp 454–7
- [10] Vaskov A K et al 2018 Cortical Decoding of Individual Finger Group Motions Using ReFIT Kalman Filter *Front. Neurosci.* **12** 3389
- [11] Collinger J L, Wodlinger B and Schwartz A B 2012 7 Degree-of-Freedom Neuroprosthetic Control By an Individual With Tetraplegia *Lancet* **381** 557–64
- [12] Hamed S B, Schieber M H and Pouget A 2007 Decoding M1 neurons during multiple finger movements *J. Neurophysiol.* **98** 327–33
- [13] Rouse A G and Schieber M H 2016 Spatiotemporal Distribution of Location and Object Effects in Primary Motor Cortex Neurons during Reach-to-Grasp *J. Neurosci.* **36** 10640–53
- [14] Nordhausen C T, Rousche P J and Normann R A 1994 Optimizing recording capabilities of the Utah Intracortical Electrode Array *Brain Res.* **637** 27–36
- [15] Serruya M D, Hatsopoulos N G, Paninski L, Fellows M R and Donoghue J P 2002 Instant neural control of a movement signal. *Nature* **416** 141–2
- [16] Gilja V et al 2012 A high-performance neural prosthesis enabled by control algorithm design *Nat. Neurosci.* **15** 1752–7
- [17] Hochberg L R et al 2006 Neuronal ensemble control of prosthetic devices by a human with tetraplegia *Nature* **442** 164–71
- [18] Pandarinath C, Nuyujukian P, Blabe C H, Soricic B L, Saab J, Willett F R, Hochberg L R, Shenoy K V and Henderson J M 2017 High performance communication by people with paralysis using an intracortical brain-computer interface *Elife* **6** 1–27
- [19] Collinger J L et al 2013 High-performance neuroprosthetic control by an individual with tetraplegia *Lancet* **381** 557–64
- [20] Bruns T M, Gaunt R A and Weber D J 2011 Multielectrode array recordings of bladder and perineal primary afferent activity from the sacral dorsal root ganglia *J. Neural Eng.* **8** 056010
- [21] Christie B P, Ashmont K R, House P A and Greger B 2016 Approaches to a cortical vision prosthesis: Implications of electrode size and placement *J. Neural Eng.* **13** 025003
- [22] Schmidt E M, Bak M J, Hambrecht F T, Kufta C V, O'Rourke D K and Vallabhanath P 1996 Feasibility of a visual prosthesis for the blind based on intracortical microstimulation of the visual cortex *Brain* **119** 507–22
- [23] Weiland J D, Cho A K and Humayun M S 2011 Retinal prostheses: Current clinical results and future needs *Ophthalmology* **118** 2227–37
- [24] Hampson R E et al 2018 Developing a hippocampal neural prosthetic to facilitate human memory encoding and recall *J. Neural Eng.* **15** 036014
- [25] Chestek C A 2011 Long-term stability of neural prosthetic control signals from silicon cortical arrays in rhesus macaque motor cortex *J. Neural Eng.* **8** 045005
- [26] Barrese J C, Rao N, Paroo K, Triebwasser C, Vargas-Irwin C, Franquemont L and Donoghue J P 2013 Failure mode analysis of silicon-based intracortical microelectrode arrays in non-human primates *J. Neural Eng.* **10** 066014
- [27] Barz F, Livi A, Lanzilotto M, Maranesi M, Bonini L, Paul O and Ruther P 2017 Versatile, modular 3D microelectrode arrays for neuronal ensemble recordings: From design to fabrication, assembly and functional validation in non-human primates *J. Neural Eng.* **14** 036010
- [28] Patel P R, Zhang H, Robbins M T, Nofar J B, Marshall S P, Kobylarek M J, Kozai T D Y, Kotov N A and Chestek C A 2016 Chronic in vivo stability assessment of carbon fiber microelectrode arrays *J. Neural Eng.* **13** 066002
- [29] Ludwig K A, Miriani R M, Langhals N B, Joseph M D, Anderson D J and Kipke D R 2009 Using a common average reference to improve cortical neuron recordings from microelectrode arrays *J. Neurophysiol.* **101** 1679–89
- [30] Stark E and Abeles M 2007 Predicting movement from multiunit activity *J. Neurosci.* **27** 8387–94
- [31] Nason S R, et al Low-power 'spiking band' feature is dominated by local single units and improves brain-machine interface performance *Nature BME* (accepted)
- [32] Kozai T D, Marzullo T C, Hooi F, Langhals N B, Majewska A K, Brown E B and Kipke D R 2010 Reduction of neurovascular damage resulting from microelectrode insertion into the cerebral cortex using in vivo two-photon mapping *J. Neural Eng.* **7** 46011
- [33] Biran R, Martin D C and Tresco P A 2005 Neuronal cell loss accompanies the brain tissue response to chronically implanted silicon microelectrode arrays *Exp. Neurol.* **195** 115–26
- [34] Holt G R and Koch C 1999 Electrical Interactions via the Extracellular Potential Near Cell Bodies *J. Comput. Neurosci.* **6** 169–84
- [35] Moffitt M A and McIntyre C C 2005 Model-based analysis of cortical recording with silicon microelectrodes *Clin. Neurophysiol.* **116** 2240–50
- [36] Anderson J M, Rodriguez A, D T Chang 2008 Foreign body reaction to biomaterials *Semin. Immunol.* **20** 86–100
- [37] Scholten K and Meng E 2015 Materials for microfabricated implantable devices: A review *Lab Chip* **15** 4256–72
- [38] Capadona J R, Shanmuganathan K, Tyler D J, Rowan S J and Weder C 2008 Stimuli-responsive polymer nanocomposites inspired by the sea cucumber dermis *Science* **319** 1370–4
- [39] Xie C, Liu J, Fu T-M, Dai X, Zhou W and Lieber C M 2015 Three-dimensional macroporous nanoelectronic networks as minimally invasive brain probes *Nat. Mater.* **14** 1286–92
- [40] Hong G, Fu T M, Zhou T, Schuhmann T G, Huang J and Lieber C M 2015 Syringe Injectable Electronics: Precise Targeted Delivery with Quantitative Input/Output Connectivity *Nano Lett.* **15** 6979–84
- [41] Fu T-M, Hong G, Zhou T, Schuhmann T G, Viveros R D and Lieber C M 2016 Stable long-term chronic brain mapping at the single-neuron level *Nat. Methods* **13** 875–82
- [42] Musk E and Neuralink 2019 An integrated brain-machine interface platform with thousands of channels *J. Med. Internet Res.* **21** 10
- [43] Zhao Z, Li X, He F, Wei X, Lin, S and Xie C 2019 Parallel, minimally-invasive implantation of ultra-flexible neural electrode arrays *J. Neural Eng.* **16** 035001
- [44] Kim B J, Kuo J T, Hara S A, Lee C D, Yu L, Gutierrez C A, Hoang T Q, Pikov V and Meng E 2013 3D Parylene sheath neural probe for chronic recordings *J. Neural Eng.* **10** 045002
- [45] Kozai T D Y, Vazquez A L, Weaver C L, Kim S-G and Cui X T 2012 Two-Photon Microscopy Reveals Immediate Microglial Reaction To Implantation of Microelectrode Through Extension of Processes *J. Neural Eng.* **9** 066001
- [46] Patel P R, Na K, Zhang H, Kozai T D Y, Kotov N A, Yoon E and Chestek C A 2015 Insertion of linear 8.4 μ m diameter 16 channel carbon fiber electrode arrays for single unit recordings *J. Neural Eng.* **12** 046009
- [47] Guitchoyts G, Markowitz J E, Liberti W A and Gardner T J 2013 A carbon-fiber electrode array for long-term neural recording *J. Neural Eng.* **10** 046016
- [48] Guitchoyts G and Cox D 2020 64-channel carbon fiber electrode arrays for chronic electrophysiology *Sci. Rep.* **10** 3830
- [49] Schwerdt H N et al 2017 Subcellular probes for neurochemical recording from multiple brain sites *Lab Chip* **17** 1104–15
- [50] Schwerdt H N et al 2017 Long-term dopamine neurochemical monitoring in primates *Proc. Natl. Acad. Sci.* **114** 13260–5

- [51] Massey T L, Santacruz S R, Hou J F, Pister K S J, Carmena J M and Maharbiz M M 2019 A High-Density Carbon Fiber Neural Recording Array Technology *J. Neural Eng.* **16** 016024
- [52] Gillis W F et al 2017 Carbon fiber on polyimide ultra-microelectrodes *J. Neural Eng.* **15** 016010
- [53] Deku F, Cohen Y, Joshi-Imre A, Kanneganti A, Gardner T and Cogan S 2018 Amorphous silicon carbide ultramicroelectrode arrays for neural stimulation and recording *J. Neural Eng.* **15** 016007
- [54] Obaid A et al 2020 Massively parallel microwire arrays integrated with CMOS chips for neural recording *Science Advances* **6** 12
- [55] Malaga K A, Schroeder K E, Patel P R, Irwin Z T, Thompson D E, Nicole Bentley J, Lempka S F, Chestek C A and Patil P G 2016 Data-driven model comparing the effects of glial scarring and interface interactions on chronic neural recordings in non-human primates *J. Neural Eng.* **13** 16010
- [56] Michelson N J and Kozai T D Y 2018 Isoflurane and ketamine differentially influence spontaneous and evoked laminar electrophysiology in mouse V1 *J. Neurophysiol.* **120** 2232–45
- [57] Green R A et al 2012 Substrate dependent stability of conducting polymer coatings on medical electrodes *Biomaterials* **33** 5875–86
- [58] Petrossians A, Whalen J J, Weiland J D and Mansfeld F 2011 Electrodeposition and characterization of thin-film platinum-iridium alloys for biological interfaces *J. Electrochem. Soc.* **158** D269–76
- [59] Cassar I R, Yu C, Sambangi J, Lee C D, Whalen J J, Petrossians A, and Grill W M 2019 Electrodeposited platinum-iridium coating improves in vivo recording performance of chronically implanted microelectrode arrays *Biomaterials* **205** 120–32
- [60] Hukins D W L, Mahomed A and Kukureka S N 2008 Accelerated aging for testing polymeric biomaterials and medical devices *Med. Eng. Phys.* **30** 1270–4
- [61] ASTM F1980 - 16 2016 Standard Guide for Accelerated Aging of Sterile Barrier Systems for Medical Devices (West Conshohocken, PA: ASTM International)
- [62] Paxinos G and Watson C 2007 The rat brain in stereotaxic coordinates (New York: Academic)
- [63] Skoglund T S, Pascher R and Berthold C H 1997 The existence of a layer IV in the rat motor cortex *Cereb. Cortex* **7** 178–80
- [64] Polikov V S, Tresco P A and Reichert W M 2005 Response of brain tissue to chronically implanted neural electrodes *J. Neurosci. Methods* **148** 1–18
- [65] Plexon Inc 2009 Offline Sorter User Guide Data Analysis Software (Dallas, Texas) Version 3
- [66] Cogan S F 2008 Neural stimulation and recording electrodes *Ann. Rev. Biomed. Eng.* **10** 275–309
- [67] Lee C D, Hudak E M, Whalen J J, Petrossians A and Weiland J D 2018 Low-impedance, high surface area Pt-Ir electrodeposited on cochlear implant electrodes *J. Electrochem. Soc.* **165** G3015–7
- [68] Neto J P, Baião P, Lopes G, Frazão J, Nogueira J, Fortunato E, Barquinha P and Kampff A R 2018 Does impedance matter when recording spikes with polytrodes? *Front. Neurosci.* **12** 1–9
- [69] Dupont S R, Novoa F, Voroshazi E and Dauskardt R H 2014 Decohesion kinetics of PEDOT:PSS conducting polymer films *Adv. Funct. Mater.* **24** 1325–32
- [70] Meyer R D, Cogan S F, Nguyen T H and Rauh R D 2001 Electrodeposited iridium oxide for neural stimulation and recording electrodes *IEEE Trans. Neural Syst. Rehabil. Eng.* **9** 2–11
- [71] Otchy T M et al 2019 Printable microscale interfaces for long-term peripheral nerve mapping and precision control (accepted) (<https://doi.org/10.1101/688218>)
- [72] Saito N, et al 2011 Application of carbon fibers to biomaterials: a new era of nano-level control of carbon fibers after 30-years of development *Chem. Soc. Rev.* **40** 3824–34
- [73] Driscoll N et al 2018 Two-dimensional Ti3C2 MXene for high-resolution neural interfaces *ACS Nano* **12** 10419–29
- [74] Luo X, Weaver C L, Zhou D D, Greenberg R and Cui X T 2011 Highly stable carbon nanotube doped poly(3,4-ethylenedioxythiophene) for chronic neural stimulation *Biomaterials* **32** 5551–7
- [75] Keefer E W, Botterman B R, Romero M I, Rossi A F and Gross G W 2008 Carbon nanotube coating improves neuronal recordings *Nat. Nanotechnol.* **3** 434–9